Kütahya Dumlupınar University
Institute of Graduate Studies

Journal of Scientific
Reports-A
E-ISSN: 2687-6167
Number 48, March 2022

RESEARCH ARTICLE

STUDYING the EFFECT of STIFFNESS VARIABILITY on SITE RESPONSE PREDICTION at LOTUNG SITE by EMPLOYING MODIFIED CAM-CLAY CONSTITUTIVE MODEL

Yusuf GÜZEL[1*]

[1]Necmettin Erbakan Üniversitesi, Mühendislik Fakültesi, İnşaat Mühendisliği Bölümü, 42500, Konya, yguzel@erbakan.edu.tr, ORCID: 0000-0003-2957-8060

Received Date:28.10.2021 *Accepted Date:22.02.2022*

ABSTRACT

Prediction of surface input motion is critical in seismic design of structures. Site response analysis through a Finite Element model can be useful in the prediction of surface input motion. The Finite Element modelling involves several uncertainties (e.g., shear wave velocity profile, shear strength, Standard penetration test values, friction angle) that will influence the predictions at the surface. This research considers the impact of shear wave velocity variability on the site response predictions under one strong and one weak input motions recorded at the Lotung site. The variability of shear wave velocity is characterized by means of Monte Carlo Simulations basing on the measured data at the site. Soil behavior is featured by Modified Cam-Clay model adapted in Finite element model, SWANDYNE. The results in terms of spectral acceleration, peak ground acceleration and shear strain profiles indicate that the stiffness variability can alter the predictions and level of this alteration depends strongly on the seismic intensity level of the input motion applied. The medians of Monte Carlo Simulation predictions are almost in line with the baseline predictions. In terms of spectral accelerations, the medians divert from the recorded data. In particular, when the strong input motion is applied, the predictions, at around the fundamental period of the soil deposit, are greater than the recorded ones. Nevertheless, the predictions express good indications to the actual values with respect to the peak ground acceleration and shear strain profiles and amplification factors.

Keywords: *Site response analysis, Stiffness variability, Monte Carlo Simulation, Spectral acceleration, Amplification factor*

JSR A
Journal of Scientific Reports

Güzel, Y., Journal of Scientific Reports-A, Number 48, 55-78, March 2022.

1. INTRODUCTION

Propagation of seismic waves through the soil deposits can greatly alter its characteristics at the surface (e.g. peak ground acceleration, PGA, peak ground displacement, PGD, peak ground velocity, PGV, bracket duration, fundamental period). This interaction between soil and seismic waves eventually influence the impact of earthquake events to the urban areas [1]. It is therefore in utmost importance to take into account main characteristics of earthquake events and soil deposits in seismic designs, in particular in seismically active regions.

One of the effective method to consider soil-seismic wave interaction is to simulate soil behaviour under earthquake input motions via analytical or numerical methods. While it is well-known that the analytical methods (e.g. EERA [2]) may lead to indicative predictions, they cannot be able to thoroughly replicate the real soil behaviours (i.e. capturing early soil nonlinearity, irreversibility, strain accumulations). In contrast, numerical methods (Swandyne [3], Plaxis [4], etc.) with soil models (Mohr-Coulomb, Modified Cam-Clay or some other advanced soil models) can be able to capture soil nonlinearity, permanent strain accumulations and built-up pore pressure. Besides, analytical methods require limited soil parameters, in use of numerical methods several sets of soil parameters may be needed, especially when advanced soil models are employed.

Main features of soil deposits, namely stiffness profile (maximum shear stiffness at minimal shear strain levels, G_{max} or shear wave velocity, V_s) and nonlinear curves or shear modulus degradation and related hysteretic damping (G/Go vs shear strain and D (%) vs shear strain) are two dominant factors in the alteration of seismic waves [5]. When the stiffness of soil deposits are measured via in-situ tests, such as cross-hole, down-hole, seismic cone, Spectral Aanalysis of Seimic Waves (SASW), suspension logging methods (e.g. [6, 7])). The nonlinear curves can be obtained up to a range of shear strains through laboratory testing of undisturbed soil samples (e.g. resonant column/torsional shear, cyclic triaxial and cyclic simple shear tests). The measured data from several studies shows that stiffness values and nonlinear curves for a site can indicate great variations, and therefore great uncertainty. For this reason, in the analysis of soil deposits these uncertainties should be taken into consideration in order to better assess the soil-seismic wave interaction. In this aspect, geotechnical arrays have become great tool in both obtaining the soil properties rigorously and analyzing the performance of the soil models by using the recorded data through the down-hole arrays. The sites instrumented by geotechnical arrays, as Gilroy, Treasure Island, Lotung and KiK-net down-hole arrays [8-12], have been focus of many studies in verification of the models and in better understanding the interaction between soil and the seismic input motions.

One way to include the variabilities is to conduct Monte-Carlo Simulation (MCS), by changing the stiffness values and nonlinear curves at each simulation within the level of variations. Li and Assimaki [13] conduct MCS at three well-investigated down-hole array sites located in the Los Angeles Basin. They use the synthetic earthquake records produced by Assimaki et.al. [14]. The results indicate that the influence of nonlinear curves variability shows huge dependency to the seismic intensity of the applied input motion, particularly in the case of soft soil profiles. In contrast, the uncertainty in stiffness demonstrates less dependency to the seismic intensity but more related to the stiffness contrast especially

at the near surface. Rathje et. al. [15] also perform MCS in equivalent linear site response analysis. In the study, along with the stiffness and nonlinear curve variabilities, the variability in the bedrock motion is considered as well. The variations of shear wave velocity profile and nonlinear curves are achieved by using the statistical model developed by Toro [16] and the model of Darendeli and Stokoe [17]. It is found that the inclusion of shear wave velocity variability causes the reduction in the median surface motions and amplification factors, pronounced strongly at periods less than the site period. Furthermore, variability of nonlinear curves has lesser impact on the surface motions. The study conducted by Guzel et. al. [18] also operates MCS for the geotechnical array site in Lotung by utilizing FE code with an advanced kinematic hardening clay model (Rouainia and Wood model [19]. The results point out that the influence of stiffness and nonlinear curve variabilities on the seismic motions depends strongly on the level of seismic motions applied. The importance of stiffness contrast near the surface on the prediction of spectral accelerations emphasized, too.

In this study, geotechnical array site in Lotung is taken into consideration. The well-documented soil deposit is modelled in a Finite Element (FE) code, Swandyne [3]. Modified Cam-Clay soil model [20] is used and only the variability of stiffness is considered via MCS with the same methodology applied in the study of Guzel et.al. [18]. One weak and one strong motions recorded along the geotechnical array at the site are simulated. Different level of stiffness variability (i.e., different level of standard deviation) is considered and their impact on the spectral accelerations, shear strain and PGA is plotted. The detail of the site and considered seismic input motions is given in the next section, followed by the introduction of stiffness variability and the result sections.

2. LOTUNG SITE AND INPUT MOTIONS

The geotechnical array formed in 1985 is located in Lotung, Taiwan. From 1985 to 1990, 30 input motions with low, moderate and high seismic intensities are recorded by accelerometers positioned at different depth of the array. The site consist of soil layers until the depth of around 47 m, sit on top of a Miocene basement. The soil deposit includes different sublayers; 17 m thick silty sand layer above a 6 m thick layer of sand with gravel resting on a stratum of silty clay interlayered by an inclusion of sand with gravel between 29 m and 36 m, as indicated by the SPT log profile reported in Fig. 1b. The level of water table is assumed to be 1 m depth below the ground surface [21].

One strong (LSST7) and one weak (LSST11) input motions are employed in order to study the effect of interaction between seismic intensity and the stiffness profile on the surface input motions. For brevity, only the East-West (EW) components of the earthquake recordings at 47 m depth are considered. Main characteristics of the earthquake events including magnitude, epicentral distance, and PGAs at the 47 m depth and at the ground surface are presented in Table 1 [6]. Corrected acceleration-time histories and corresponding spectral accelerations are plotted in Figure 2. As clearly seen, strong motion has seismic energy at long durations and thus at high periods while weak motion has relatively low energy and duration. This is typical features of strong and weak input motions. The frequency contents of earthquake input motions reflects the seismic waves within various frequencies and amplitudes. The strong input motion can have high amplitudes at lower frequencies when the weak input motion can have high amplitudes at lower frequency levels.

JSR A
Journal of Scientific Reports

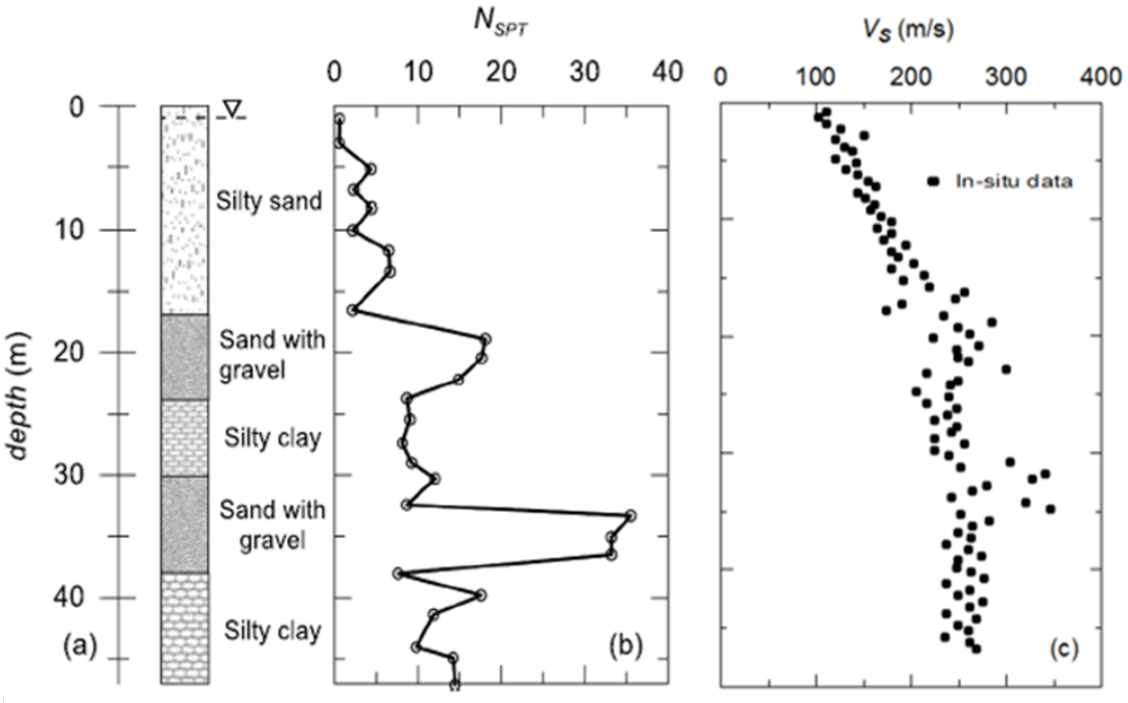

Figure 1. (a) Stratigraphy, (b) SPT log at the LSST site and c) measured shear wave velocity (V_s) profile along the depth of 47 m.

Table 1. Earthquakes recorded by the LSST array and simulated in the analyses [18].

Event	**Date**	**M_L**	**Epicentral distance (km)**	**Focal depth (km)**	**PGA (g) at 47 m depth**			**PGA (g) at the surface**		
					E-W	**N-S**	**V**	**E-W**	**N-S**	**V**
LSST07	20.5.1986	6.2	66.0	15.8	0.080	0.093	0.030	0.160	0.210	0.040
LSST11	17.7.1986	4.3	6.0	2.0	0.046	0.060	0.015	0.070	0.100	0.040

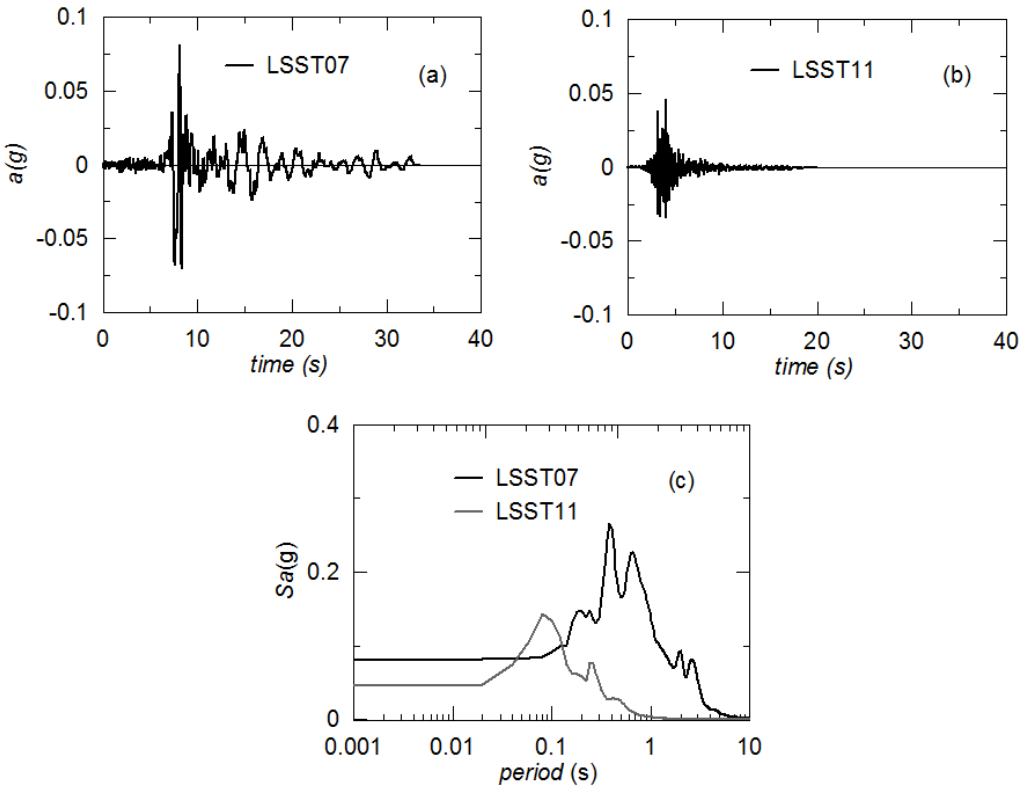

Figure 2. Recorded input motions at the Lotung site in the East-West (E-W) direction: (a) strong earthquake event (LSST7), (b) weak earthquake event (LSST11) and corresponding spectral accelerations.

3. SOIL PARAMETERS

The Modified Cam-Clay (MCC) model has been implemented in SWANDYNE II, which is a full-coupled finite element code solving the wave propagation problem in the time domain and enabling to model the soil deposit in two or three-dimensional spaces. Linear or nonlinear dynamic analyses can be performed, using the Generalised Newmark method [22] for time integration. Compression and swelling index parameters of the soil model, λ and κ, are obtained from odometer test results [6] as presented in Table 2. The value of Poisson's ratio is taken equal to 0.46 constant with depth due to the $K0$ value of 0.85, which is adjusted with respect to the predictions of the recorded pore water pressure during November 15, 1986 earthquake event (proposed by Li *et al.* [23] and Berger *et al.* [24]).. M, the slope of the critical state line, is calculated from friction angle predictions obtained from measured SPT-N values by using the following empirical formulation [25]:

$\emptyset_d=(20N)^{0.5}+18$ (1)

$M=6(\sin\emptyset-3)/\sin\emptyset$ (2)

In this study, the well-known equation proposed by Viggiani and Atkinson [26] for the small-strain shear modulus has been used to reproduce the dependency of G_0 on the mean effective stress and over-consolidation ratio:

$$\frac{G_o}{p_r} = A\left(\frac{p'}{p_r}\right)^n OCR^m \quad (3)$$

where p_r is a reference stress taken as 1 kPa, p' is mean effective stress, *OCR* is the over-consolidation ratio defined in terms of mean effective stress, *A*, *m* and *n* are the soil plasticity index (*PI*) dependent stiffness parameters. The best-fit G_0 profile in Figure 3a is achieved with *A*, *m* and *n* parameters shown in Table 2. In addition, OCR is considered 4 from 0 to 6 m depth and for the remaining soil profile a constant value of 2 is defined. These OCR values ensures that the calculated G_0 profile fits well with the G_0 values depicted from measured V_s values. 3% of Rayleigh damping is introduced in order to dissipate energy at the small strain levels as suggested by Kwok et.al. [26].

Table 2. Soil model parameters for different soil layers.

Depth	λ	κ	*M*	*υ*	*A*	*m*	*n*
0-17 m	0.0066	0.0015	0.922	0.46	1000	0.36	0.82
17-23 m	0.0066	0.0015	1.096	0.46	1900	0.36	0.82
23-29 m	0.0066	0.0015	0.814	0.46	1350	0.36	0.82
29-36 m	0.0066	0.0015	0.941	0.46	1900	0.36	0.82
36-47 m	0.0066	0.0015	0.730	0.46	1150	0.36	0.82

4. VARIATION IN THE INITIAL STIFFNESS PROFILE

The shear wave velocity values along the 47 m depth of the LSST site are attained from the in-situ test results (i.e. seismic cross-hole and up-hole tests) and presented in Figure 3. Recalling the Eq 3 adopted in the FE procedure for the small-strain shear modulus (G_0) profile of the Lotung site:

$$\frac{G_o}{p_r} = A\left(\frac{p'}{p_r}\right)^n OCR^m$$

For a soil layer, p', p_r and OCR are regarded as constant, only the A, m and n parameters are options for the variation of the stiffness. In this respect, m and n parameters are costumed as determinant with values of 0.36 and 0.82, respectively, given the reason that they have relatively narrow scale of values and, thus, has minor effect on the stiffness computation. Therefore, only the randomisation of A parameter is considered in producing stiffness profiles for the MCSs. In particular, a point variability is considered here, i.e. the initial stiffness profile is truncated from the baseline profile with the specified levels of standard deviation. Assuming the A parameter (and so the G_0 values) is lognormally distributed, reasonable fit with the measured values are attained for different soil layers, as shown in Figure 3a. Moreover, by using the lognormal distribution, stiffness values to being positive is assured [27]. The average G_0 profile with depth presented in Figure 3 represents the baseline profile used in the baseline predictions. It is important to note here that the formulation in randomization of the stiffness profile is the same with the one applied in the study of Guzel et.al. [18].

When only the A parameter is random, the mean and standard deviation of G_0 are:

$$\mu_{G_o} = \mu_A\left(\frac{p'}{p_r}\right)^n OCR^m$$

$$\sigma_{G_o} = \mu_A COV_A\left(\frac{p'}{p_r}\right)^n OCR^m \quad (4)$$

Since the stress and overconsolidation ratio dependency of G_0 is sustained in the calculation of the mean and standard deviation, the coefficient of variance (*COV*) of G_0 can be computed as:

$$COV_{G_o} = \frac{\sigma_{G_o}}{\mu_{G_o}} = COV_A \quad (5)$$

meaning that the *COV* is kept constant in the transformation of *A* into G_0.

After ensuring the consistency in the *COV*, it is necessary to calculate the statistical parameters of the lognormal distribution, e.g. the mean and standard deviation. The calculation of these parameters, along with the probability density function (PDF) of *A*, is given as:

$$A: \ln(\mu_{lnA}, \sigma_{lnA}) = exp(\mu_{lnA} + \sigma_{lnA} \times \xi) \quad (6)$$

where, $\xi \sim N(0,1)$ is a normally distributed random variable.

$$\mu_{lnA} = ln\left(\frac{\mu_A}{\sqrt{1+COV_A^2}}\right) \tag{7}$$

$$\sigma_{lnA} = \sqrt{ln(1+COV_A^2)}$$

Once the PDF expression of A (i.e. Eqç 6) is substituted into Eqç 3, G_0 can be written as follows:

$$G_o = exp(\mu_{lnA} + \sigma_{lnA}\xi)p'\left(\frac{p'}{p_r}\right)^n OCR^m \tag{8}$$

Reforming the expression given above:

$$G_o = \exp(\mu_{lnA} + (1-n)p_r + nln(p') + mln(OCR) + \sigma_{lnA}\xi) \tag{9}$$

From this formulation, the transformation of variability from A to G_0 only affects the mean of lnG_0 when a certain desired variability is given by the standard deviation [28]. Then, the log-normally distributed G_0 can be given as:

$$G_o : \ln\left(\mu_{lnG_o}, \sigma_{lnG_o}\right) \tag{10}$$

and:

$$\mu_{lnG_o} = \mu_{lnA} + (1-n)p_r + nln(p') + mln(OCR) \tag{11a}$$

$$\sigma_{lnG_o} = \sigma_{lnA} \tag{11b}$$

When, at the end of these steps, the G_0 profile is randomized, the variation in the associated V_s profile with depth is ensured with the assumption of a total unit weight of 20 kN/m^3 (as proposed by Borja *et al.* [29]). One single realisation of shear wave velocity profiles adapted in this research is demonstrated in Figure 3.

JSR A
Journal of Scientific Reports

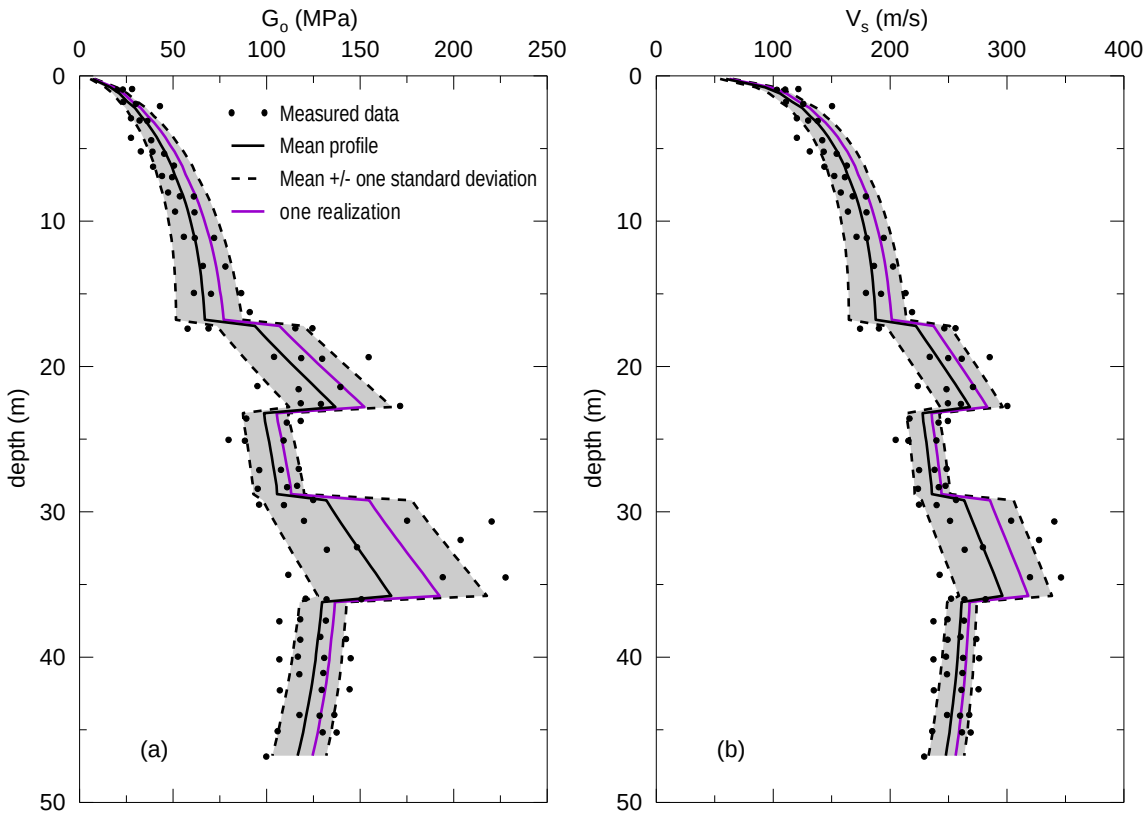

Figure 3. Point variability of stiffness: (a) shear modulus (G_0) profile and (b) shear wave velocity profile (V_s).

5. RESULTS

5.1. Influence of Stiffness Variability under Weak Input Motion

The spectral accelerations of recorded input motions at bedrock and ground level are plotted in Figure 4 along with the MCS their median and baseline responses. The presented baseline response is obtained by using the mean stiffness profile. 1_std, 2_std and 3_std truncations imply the results for V_s profiles produced within plus/minus one, two and three levels of standard deviation from the median profile.

It is clear that the actual bedrock input motion experience great amplification and period elongation due to soil nonlinearity when it travels through the surface. MCS results also exhibit considerable increase of

JSR A
Journal of Scientific Reports

spectral accelerations at 1std, 2std and 3std truncation levels (Figure 4a, b, and c, respectively). While the first peak is reasonably well captured, the main peak occurring around the fundamental period of the soil deposit (i.e., T_1, equals to 0.85 second) is taken place at earlier periods. Nevertheless, in all cases predicted Sa between 0 and 0.12 period ranges overlaps almost fully with the recorded values. At medium period ranges (between 0.12 s and 1 s), baseline prediction and MCS predictions are bigger than the recorded ones. Over 1 s, predictions are always smaller than the actual spectral accelerations.

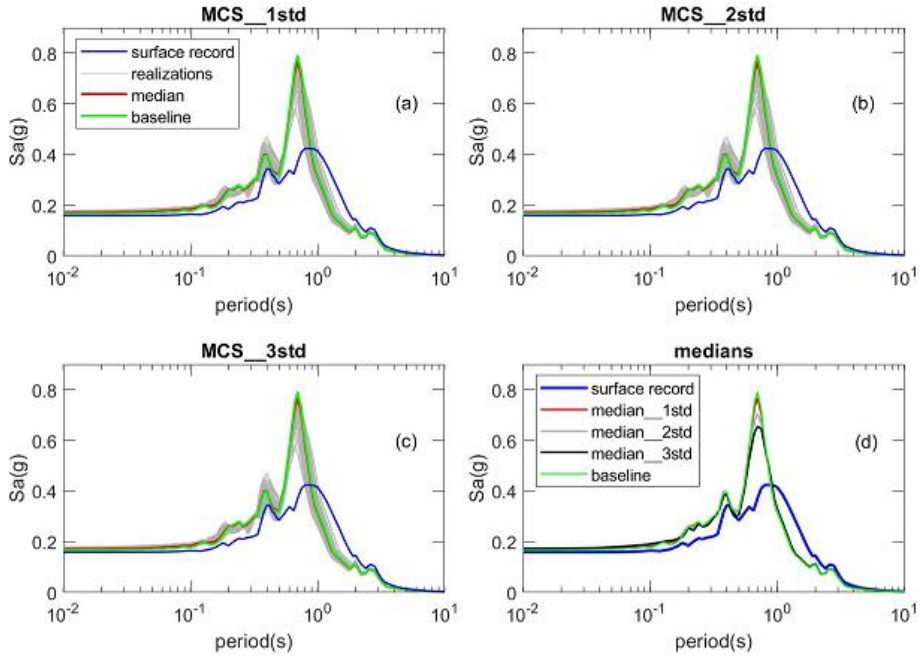

Figure 4. Spectral acceleration predictions from MCSs, under LSST7EW earthquake input motion, along with median, baseline and surface and bedrock input motions with; (a) 1std level of truncation, (b) 2std level of truncation and (c) 3std truncations and (d) comparison of medians from three cases of truncation.

Variation in the spectral acceleration predictions are mainly happen at 0.12 s and 2.5 s period interval, while at lower and higher periods seems to be insignificant in all truncation levels observed. Introduction of stiffness variability causes inconsiderable changes in the median spectral response when 1std level of truncation is considered (Figure 4d). In contrast, when 2 or 3std levels of truncation are utilized, predicted median spectral response reduces, in particular at around T_1. This can be attributed to the fact that the impact of soil behaviour on the input motion is pronounced more at T_1. Because, the soil deposit tends to oscillate more at its period ranges, therefore the stiffness variability leads to more changes within that period ranges in spectral acceleration predictions than at other periods. This can be seen in the lognormal standard deviation levels of MCS predictions (the reason in considering lognormal standard deviation is

spectral acceleration at a single period is considered to be lognormally distributed as stated by Assimaki et.al. [5].

As can be seen in Figure 7, the levels of standard deviation at around T_1 are higher than at other periods in all three cases. Besides, increasing the level of truncation from 1 to 3std, as expected, introduces more uncertainty, since the standard deviation at all periods become higher with the increment of truncation level (Figure 7a). The maximum standard deviation is 0.14 when the stiffness is varied at 1std level of truncation while it is 0.22 and 0.29 in 2std and 3std levels of truncation, respectively. Figure 5 and 6 values. demonstrate the PGA and shear strain profiles of MCSs along 47 m depth, respectively). It is clear that the predicted PGA values are bigger than the recorded ones at 17 and 11 m depths. At 6 m and at the surface they are relatively matched well in all three truncation levels. Increasing the level of truncation from 1std to 2std and 3std has small effect on the predicted median profiles of PGA (Figure 5d and Figure 6d) and shear strain but only introduce more variability as it leads to increase in the level of standard deviations (Figure 7b and 7c). In addition, median profiles of PGA and shear strain are in good agreement with the baseline predictions, especially at the near surface. From both PGA and shear strain profiles, different soil layers, characterised by different stiffness values, can easily be recognised. As the sand layers with gravel include relatively greater shear wave velocity, higher level of PGA and shear strains are developed. However, within these soil layers greater level of uncertainty is observed, in particular at the borders of the layers exhibiting dramatic changes of PGA and shear strain values. This may be attributed to the level of stiffness contrast between soil layers. While within a soil layer there is a tendency in both PGA and shear strain profiles showing smooth increments, the transition from one oil layer to another express large changes of PGA and strain. This becomes more explicit with the increment of the truncation levels.

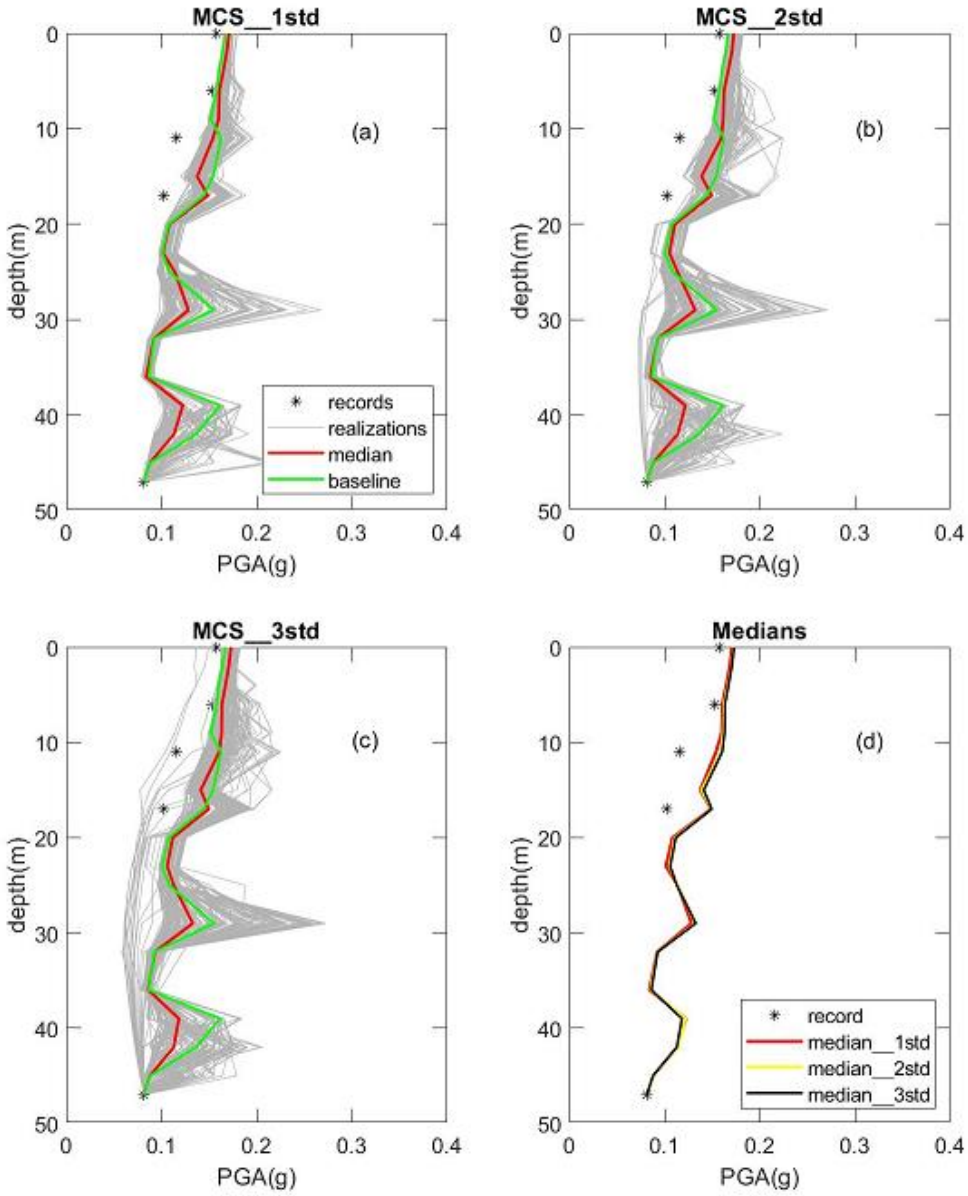

Figure 5. PGA profiles from MCSs, under LSST7EW earthquake input motion, along with median, baseline and recordings with ; (a) 1std level of truncation, (b) 2std level of truncation and (c) 3std truncations and (d) comparison of medians from three cases of truncation.

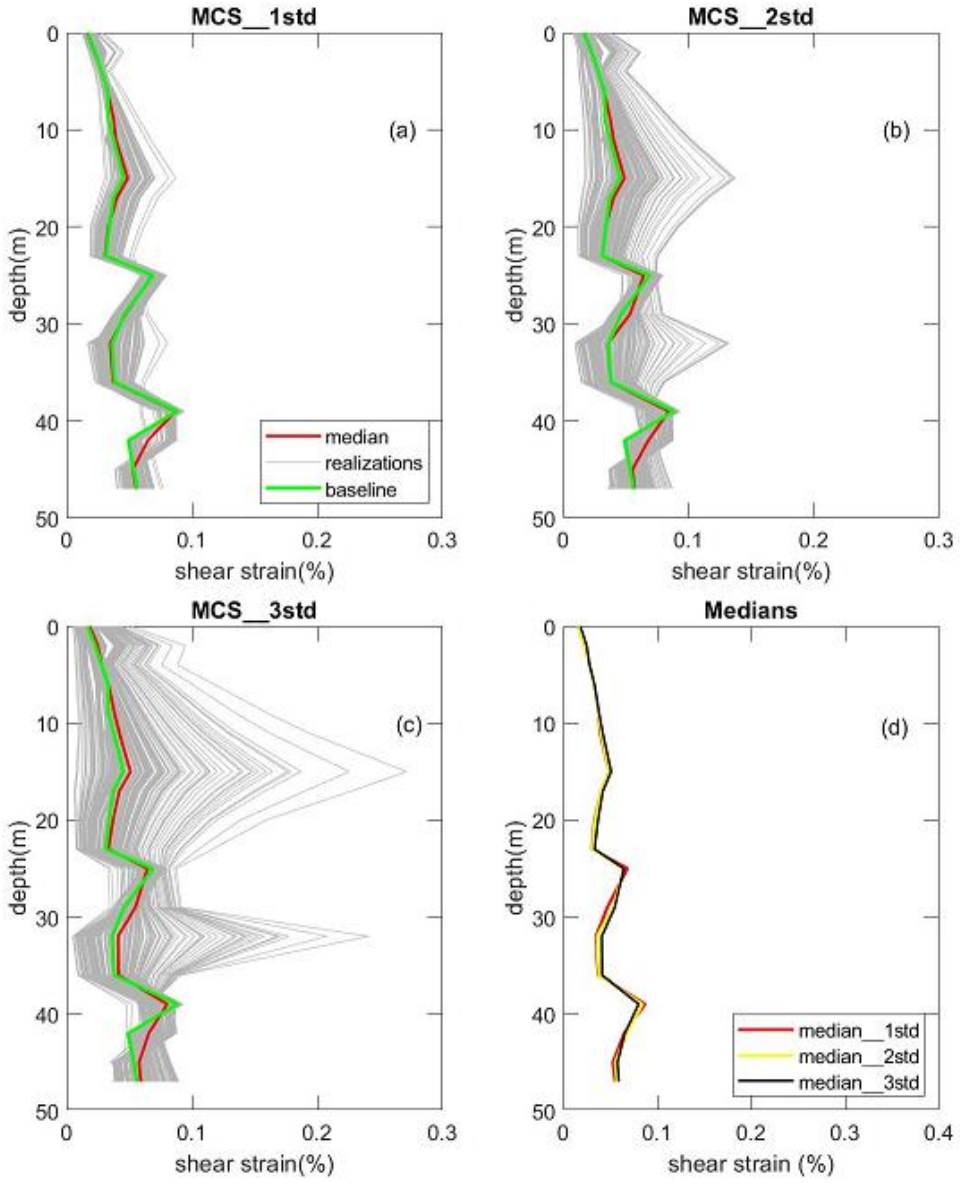

Figure 6. Shear strain profiles from MCSs, under LSST7EW earthquake input motion, along with median and baseline with ; (a) 1std level of truncation, (b) 2std level of truncation and (c) 3std truncations and (d) comparison of medians from three cases of truncation.

JSR A
Journal of Scientific Reports

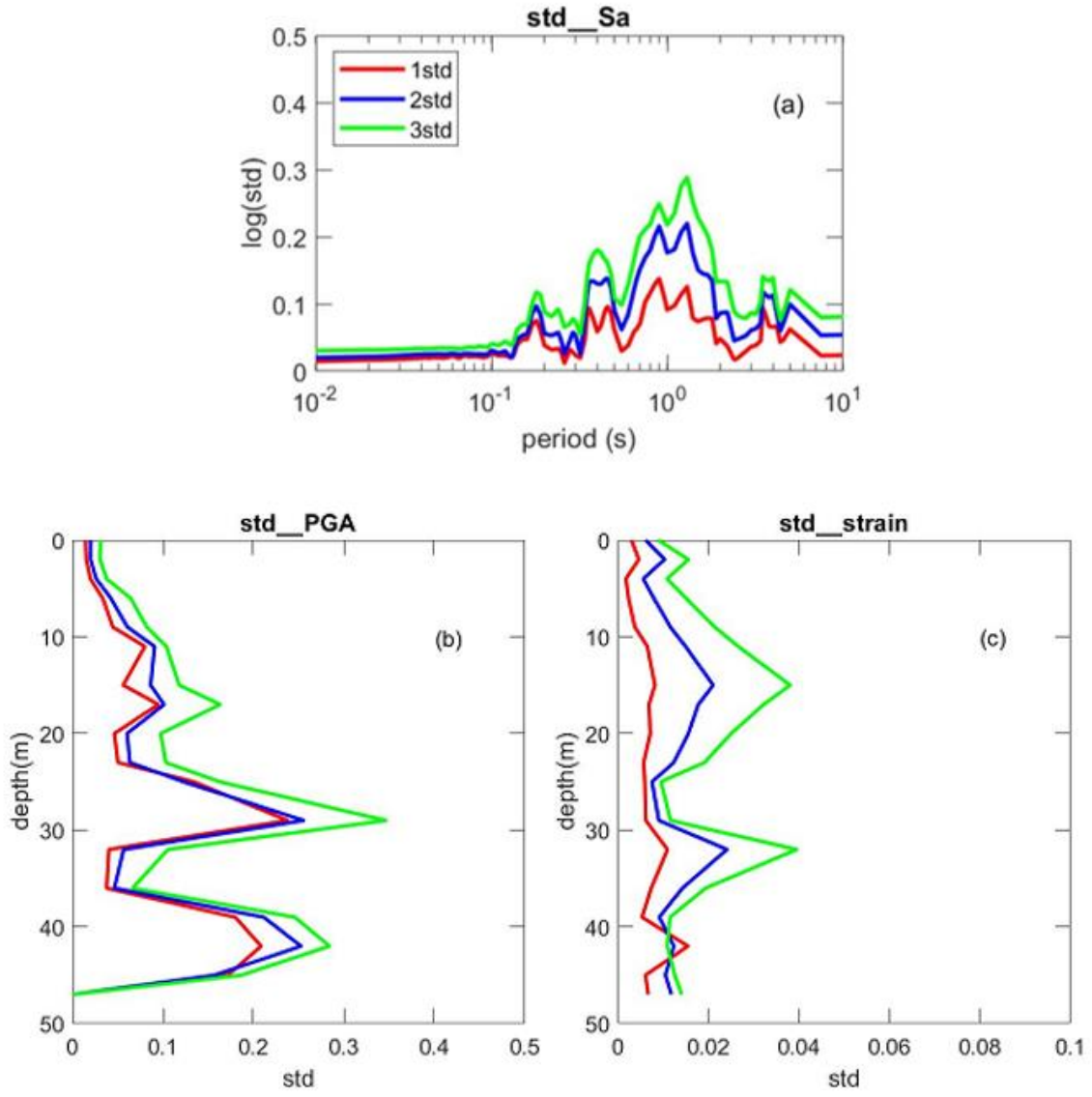

Figure 7. Level of standard deviations in three different truncation levels for; (a) spectral acceleration, (b) PGA profile and (c) shear strain profile predictions, under LSST7EW earthquake input motion.

5.2. Influence of Stiffness Variability under Weak Input Motion

In contrast to the strong input motion cases, where small effect of stiffness variability is observed at periods other than the 0.12 s and 0.25 s ranges, the stiffness variability tends to affect considerably the spectral accelerations at periods from 0 s to 1.6 s (Figure 8). Introduction of higher level of std (or truncation), leads to trivial changes in the median spectral accelerations until 0.2 s, where predicted values are always below the baseline and actual spectral accelerations, as can be seen in Figure 8d. From 0.2 s to 1.6 s, medians at three different truncation levels are always greater than the baseline and real spectral accelerations.

Increase of truncation levels from 1std to 2std and 3std, at this period range, causes medians to be closer to the real spectral accelerations while baseline prediction suits well with the actual ones. Again, the increase of truncation levels tends to raise the level of standard deviations of MCSs up to 1.6 s and above 2 s (see Figure 11a), between these two periods, the level of standard deviations induced by the level of truncation become mostly identical. In respect to the PGA and shear strain profiles, the medians of MCSs, presented in Figure 9 and 10, are almost the same at all three truncation levels and they are also in good agreement with the recorded PGA values at 17 m, 11 m, 6 m and at the surface level (Figure 9d and 10d). The rise in the level of standard deviations over the soil profile exhibit, similarly, rising trend of standard deviations for PGA, especially at the near surface as can be observed in Figure 9. This is due to the fact that the soil induces relatively greater nonlinearity at the near surface, hence the PGA values tends to show more sensitivity to the level of stiffness uncertainty. This is not valid for the shear strain profile as the standard deviation levels are similar from bottom to the 17 m depth (Figure 11c). At the top 17 m, 2std level of truncation expresses the least standard deviation; while it is lesser in case of 3std level of truncation than in case of 2std level of truncation.

It is important to note here that the soil layers are clearly differentiated between each other when the shear strain profiles are seen in Figure 10a-b-c, similar to the case under the strong input motion. However, the PGA profiles do not particularly show such trend as the PGA values along the soil deposit are smoothly transmitted from one layer to the other. This might be the indication of lesser effect of stiffness contrast on the PGA values when the weak input motion is involved.

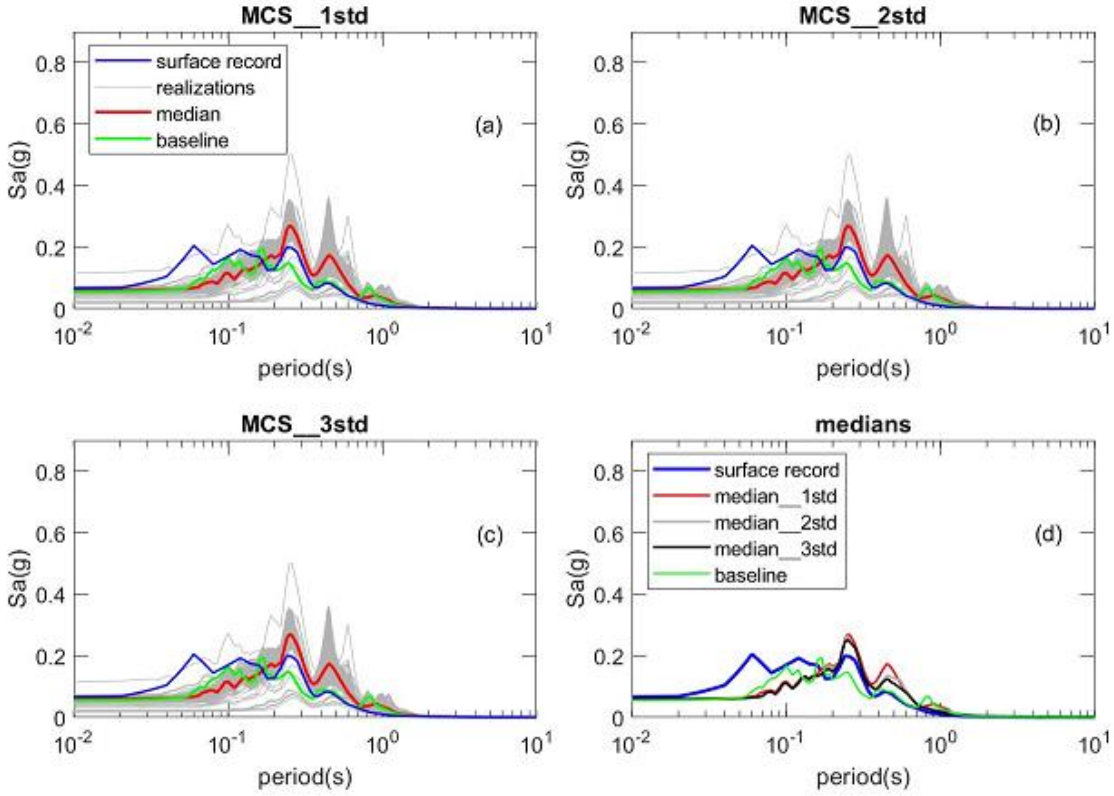

Figure 8. Spectral acceleration predictions from MCSs, under LSST11EW earthquake input motion, along with median, baseline and surface and bedrock input motions with; (a) 1std level of truncation, (b) 2std level of truncation and (c) 3std truncations and (d) comparison of medians from three cases of truncation.

JSR A
Journal of Scientific Reports

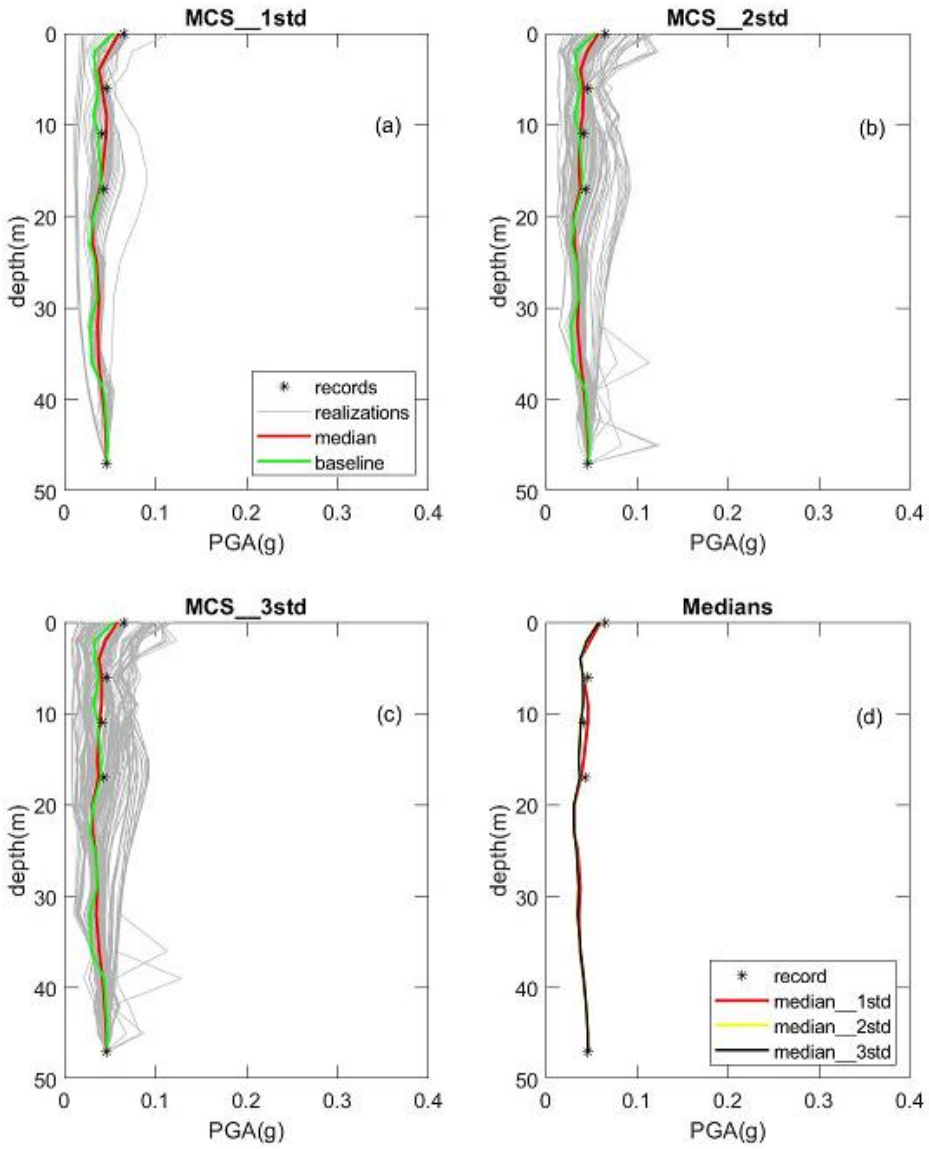

Figure 9. PGA profiles from MCSs, under LSST11EW earthquake input motion, along with median, baseline and recordings with ; (a) 1std level of truncation, (b) 2std level of truncation and (c) 3std truncations and (d) comparison of medians from three cases of truncation.

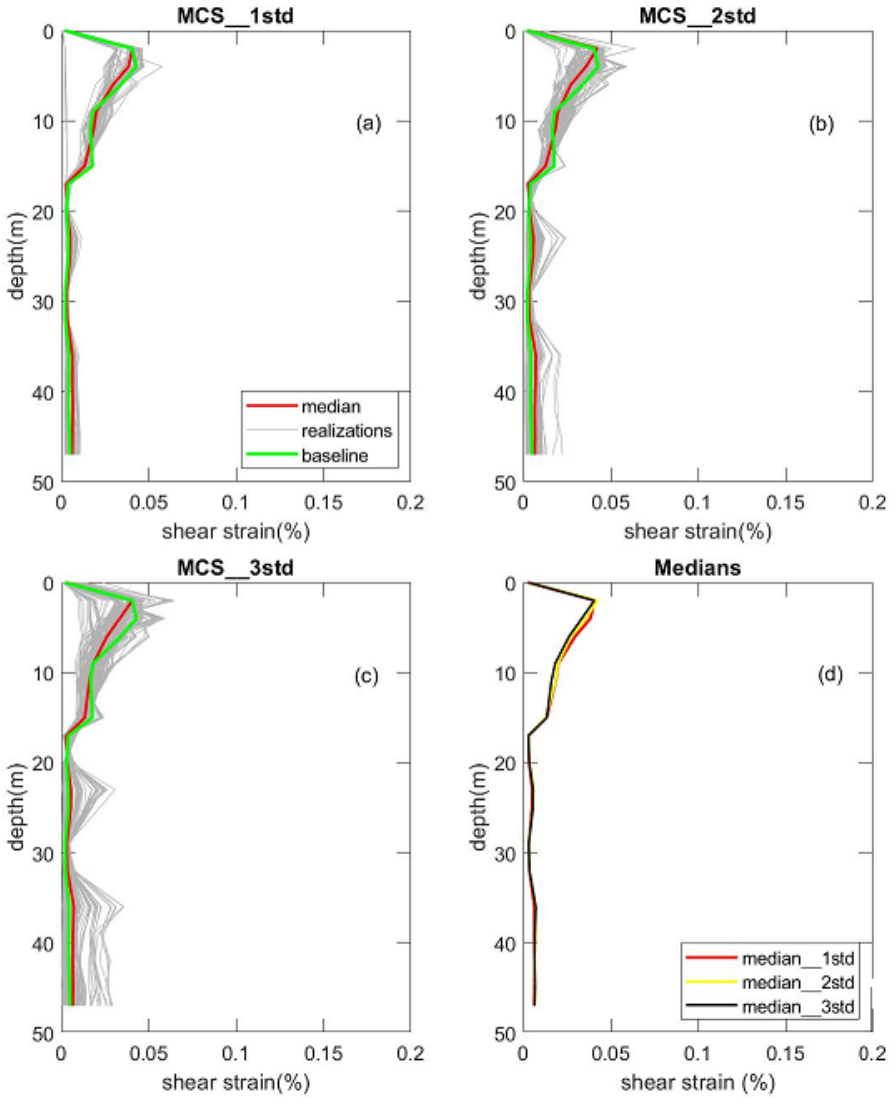

Figure 10. Shear strain profiles from MCSs, under LSST11EW earthquake input motion, along with median and baseline with ; (a) 1std level of truncation, (b) 2std level of truncation and (c) 3std truncations and (d) comparison of medians from three cases of truncation.

JSR A
Journal of Scientific Reports

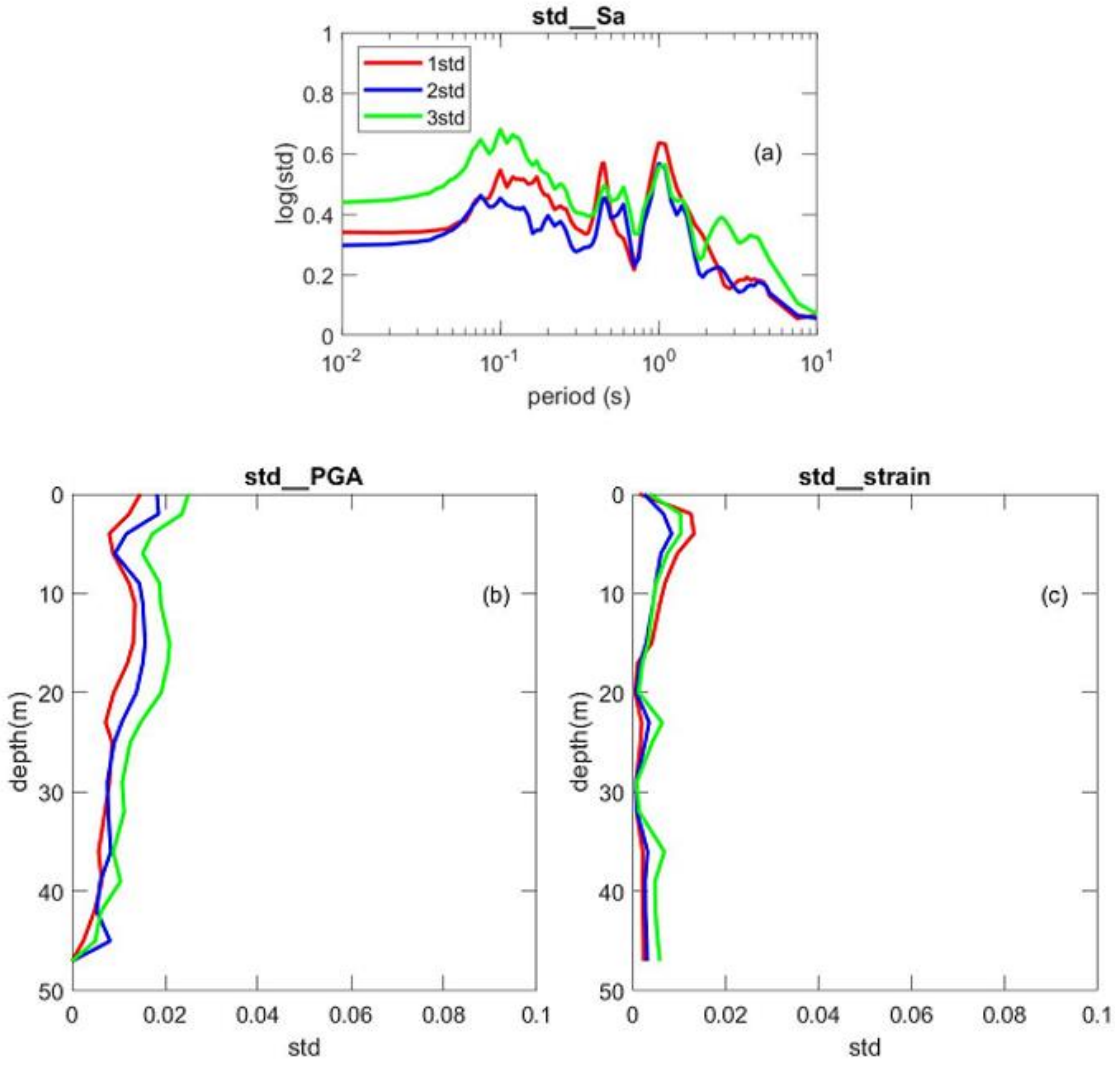

Figure 11. Level of standard deviations in three different truncation levels for; (a) spectral acceleration, (b) PGA profile and (c) shear strain profile predictions, under LSST7EW earthquake input motion.

5.3. Amplification Factors for Strong and Weak Input Motions

Amplification factor plots for medians of MCSs, baseline and actual one (under strong input motion) shows good agreement from 0 s to 0.18s while between 0.18s and 0.9s predicted values are almost

identical and higher than the actual values (see Figure 12a). Above 0.9 s, the trend inverses by predicted values becoming smaller than the actual ones. Amplification factors presented in Figure 12a for medians of MCSs and baseline profile cannot be able to capture the time of the spectral peak of strong input motion as it is previously observed in their spectral acceleration plots (i.e., Figure 4). Nevertheless, the magnitude of maximum amplification factors, from baseline profile, 1std and 2std truncation levels, agree well with the actual one, which is around 3.5 (Figure 12a). In the case of 3std truncation level, the value of maximum amplification factor is only 3.15.

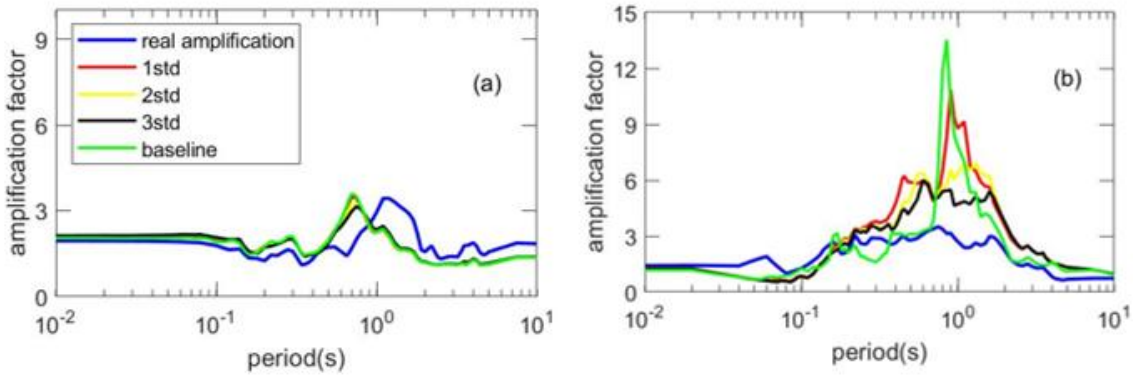

Figure 12. Comparison of amplification factors for medians of MCSs at three different level of truncations along with baseline and real amplifications over the period of interest under; (a) strong input motion (b) weak input motion.

Figure 12b represents the same plots under the weak input motion. When the real amplification factor plot is relatively smooth (due to characteristics of a weak motion carrying seismic energy at high frequencies), the ones for baseline and 1std truncation level have sharp spectral peaks with greater level of overestimations, precisely 3.51 for actual maximum amplification followed by 13.5 and 10.1, respectively. In case of 2 and 3std truncation levels, figures become smoother with the maximum magnitudes of 6.9 and 6, and get closer to the actual value of 3.51. Hence, it can be said that the increment in the level of truncation leads to better estimation of the spectral amplification, but still two times greater than the actual value.

6. CONCLUSIONS

This study focuses on the impact of stiffness (i.e., shear wave velocity) variability on site response predictions at the downhole array site in Lotung, Taiwan. Well-documented site is modelled within the FE model (SWANDYNE) by employing Modified Cam-Clay model. One strong and one weak input motions recorded at the bedrock level of the site are considered. Stiffness variability is introduced through the Monte Carlo Simulations based on the shear wave velocity data measured at the site. The spectral

accelerations and amplification factors at the surface, PGA and shear strain profiles are the interested results of discussions. The results can be outlined as followings;

- Stiffness variability shows considerable effect on the spectral acceleration predictions at around T_1 when the strong input motion is applied. In case of the weak input motion, such effect is observed over the ranges of periods. Therefore, the impact is dependent of the level of the input motion.

- Secondly, medians of MCSs under strong input motion does not clearly distinguish from each other and from baseline prediction, apart from around T_1. In addition, predicted spectral peaks occur at around T_1 and are greater than the actual peak. When the weak motion is in place, the medians are also closely matched.

- Increasing the level of truncation leads to more uncertainty but does not necessarily improves the results of spectral accelerations and PGA and shear strain profiles.

- While the effect of stiffness contrast between the soil layers are obvious in the case of strong input motion, such impact is not observed under the weak input motion.

- Predicted amplification factors indicate sufficient proxy to the actual one for the strong input motion. While this is not valid for the weak input motion, increasing the truncation level improves such prediction, though still not good enough.

Overall, the performance of MCC model is satisfying in the sense that it leads to good indication of spectral accelerations and, particularly, amplification factors. Involvement of stiffness variability through the MCSs is not necessary. Based on this study, further research is needed to characterize stiffness contrast between soil layers leading to better understanding of transformation of the input motions towards the surface.

ACKNOWLEDGEMENT

There is no funding body the author could acknowledge.

REFERENCES

[1] Ramos-Sepúlveda, M. E., & Cabas, A. (2021). Site Effects on Ground Motion Directionality: Lessons from Case Studies in Japan. Soil Dynamics and Earthquake Engineering, 147, 106755.

[2] Bardet, J.P., Ichii, K. and Lin, C.H. (2000). EERA: a computer program for equivalent-linear earthquake site response analyses of layered soil deposits. University of Southern California, Department of Civil Engineering.

[3] Chan, A.H.C. (1995). 'User's Manual for DIANA-SWANDYNE II. University of Birmingham, UK.

[4] Brinkgreve, R.B.J., Kumarswamy, S., Swolfs, W.M., Waterman, D., Chesaru, A. and Bonnier, P.G., 2016. PLAXIS 2016. *PLAXIS* bv, the Netherlands.

[5] Assimaki, D., Li, W., Steidl, J. and Schmedes, J. (2008). Quantifying nonlinearity susceptibility via site-response modeling uncertainty at three sites in the Los Angeles Basin. Bulletin of the Seismological Society of America, 98(5), 2364-2390.

[6] EPRI (1993). Guidelines for determining design basis ground motions-Volume 1: method and guidelines for estimating for estimating earthquake ground motion in Eastern North America. Rep. No. TR-102293. Palo Alto, California: Electric Power Research Institute.

[7] Kramer, L.S. (2014) *Geotechnical Earthquake Engineering*. Essex, England: Pearson Education Limited.

[8] Kaklamanos, J., Baise, L.G., Thompson, E.M. and Dorfmann, L. (2015). Comparison of 1D linear, equivalent-linear, and nonlinear site response models at six KiK-net validation sites. Soil Dynamics and Earthquake Engineering, 69, 207-219.

[9] Elia, G., Rouainia, M., Karofyllakis, D. and Guzel, Y. (2017). Modelling the non-linear site response at the LSST down-hole accelerometer array in Lotung. Soil Dynamics and Earthquake Engineering, 102, 1-14.

[10] Amorosi, A., Boldini, D. and di Lernia, A. (2016). Seismic ground response at Lotung: Hysteretic elasto-plastic-based 3D analyses. Soil Dynamics and Earthquake Engineering, 85, 44-61.

[11] Park, D., & Hashash, Y. M. (2004). Soil damping formulation in nonlinear time domain site response analysis. Journal of Earthquake Engineering, 8(02), 249-274.

[12] Darragh, R. B., & Idriss, I. M. (1997). A Tale of Two Sites: Gilroy# 2 and Treasure Island: Site Response Using an Equivalent-linear Technique. Earthquake Engineering Research Institute.

[13] Li, W., & Assimaki, D. (2010). Site-and motion-dependent parametric uncertainty of site-response analyses in earthquake simulations. Bulletin of the Seismological Society of America, 100(3), 954-968.

[14] Assimaki, D., Li, W., Steidl, J. and Schmedes, J. (2008). Quantifying nonlinearity susceptibility via site-response modeling uncertainty at three sites in the Los Angeles Basin. Bulletin of the Seismological Society of America, 98(5), 2364-2390.

[15] Rathje, E.M., Kottke, A.R. and Trent, W.L. (2010). Influence of input motion and site property variabilities on seismic site response analysis. Journal of Geotechnical and Geoenvironmental Engineering, 136(4), 607-619.

[16] Toro, G. R. (1995). Probabilistic models of site velocity profiles for generic and site-specific ground-motion amplification studies. Technical Rep. No. 779574. Brookhaven National Laboratory, Upton, New York.

[17] Darendeli, M.B., Stokoe, K.H. (2001). Development of a new family of normalized modulus reduction and material damping curves. Geotech. Engrg. Rpt. GD01-1. Austin: University of Texas.

[18] Guzel, Y., Rouainia, M. and Elia, G. (2020). Effect of soil variability on nonlinear site response predictions: Application to the Lotung site. Computers and Geotechnics, 121, 103444.

[19] Rouainia, M., & Muir Wood, D. (2000). A kinematic hardening constitutive model for natural clays with loss of structure. Géotechnique, 50(2), 153-164.

[20] Roscoe, K. and Burland, J.B. (1968). On the generalized stress-strain behaviour of wet clay.

[21] Anderson, D.G. and Tang, Y.K. (1989). Summary of soil characterization program for the Lotung large-scale seismic experiment. Proc. EPRI/NRC/TPC workshop on seismic soil-structure interaction analysis techniques using data from Lotung, Taiwan, EPRI NP-6154, 1, 4.1, 4.20. Palo Alto: Electric Power Research Institute.

[22] Katona, M.C. and Zienkiewicz, O.C. (1985). A unified set of single step algorithms part 3: The beta-m method, a generalization of the Newmark scheme. International Journal for Numerical Methods in Engineering, 21(7), 1345-1359.

[23] Li, X.S., Shen, C.K. and Wang, Z.L. (1998). Fully coupled inelastic site response analysis for 1986 Lotung earthquake. Journal of Geotechnical and Geoenvironmental Engineering, 124(7), 560-573.

[24] Berger E., Fierz H., Kluge D. (1989). Predictive response computations for vibration tests and earthquake of May 20, 1986 using an axisymmetric finite element formulation based on the complex response method and comparison with measurements-a Swiss contribution. In: Proceedings of the EPRI/NRC/TPC workshop on seismic soil-structure interaction analysis techniques using data from Lotung, Taiwan, EPRI NP-6154, vol 2, 15.1–15.47. Palo Alto: Electric Power Research Institute.

[25] Hatanaka, M. and Uchida, A. (1996). Empirical Correlation between Penetration Resistance and Internal Friction Angle of Sandy Soils. Soils and Foundations, 36(4), 1-9.

[26] Kwok, A.O., Stewart, J.P., Hashash, Y.M., Matasovic, N., Pyke, R., Wang, Z. and Yang, Z. (2007) Use of exact solutions of wave propagation problems to guide implementation of nonlinear seismic ground response analysis procedures. Journal of Geotechnical and Geoenvironmental Engineering, 133(11), 1385-1398.

[27] Andrade, J.E. and Borja, R.I. (2006). Quantifying sensitivity of local site response models to statistical variations in soil properties, Acta Geotechnica, 1(1), 3-14.

[28] Depina, I., Le, T.M.H., Eiksund, G. and Benz, T. (2015). Behavior of cyclically loaded monopile foundations for offshore wind turbines in heterogeneous sands. Computers and Geotechnics, 65, 266-277.

[29] Borja, R.I., Chao, H.-Y., Montáns, F.J. and Lin, C.-H. (1999). Nonlinear ground response at Lotung LSST site', Journal of Geotechnical and Geoenvironmental Engineering, 125(3), 187-197.